Centre bow and wet-deck design for motion and load reductions in wave piercing catamarans at medium speed

Babak Shabani[1], Jason Lavroff[1], Damien S Holloway[1], Michael R Davis[1], and Giles A Thomas[2]

[1] *School of Engineering, University of Tasmania, Hobart, TAS 7001, Australia*

[2] *Department of Mechanical Engineering, University College London, UK*

Corresponding author: babak.shabani@utas.edu.au

ABSTRACT

For wave piercing catamarans (WPCs), the centre bow length and tunnel clearance are important design factors for slamming, passenger comfort and deck diving. An experimental study was performed here to determine the influence of centre bow and wet-deck geometry on WPC motions and loads. The vertical accelerations, magnitudes of slamming loads and vertical bending moments acting on a 112 m WPC vessel were investigated at a reduced speed of 20 knots using five centre bow (CB) and wet-deck configurations: parent CB, high CB, low CB, long CB and short CB. A 2.5 m hydroelastic segmented catamaran model was used and over 200 model tests were conducted in regular head sea waves in wave heights equivalent to 2.7 m, 4.0 m and 5.4 m at full scale. It was found that increasing the wet-deck height resulted in higher vertical accelerations due to global motions but reduced the slamming loads at a speed of 1.53 m/s in model scale (20 knots full scale). The greatest peak vertical loads acting on the centre bow ranged between 18% and 105% of the total hull weight depending on the centre bow configuration and wave height. Correlation coefficients were obtained for regression models describing the relationship between the total vertical loads and the peak vertical bending moments. It was found that a reduction of speed from 38 knots to 20 knots can reduce the maximum slam loads by approximately 30% in regular waves. When considering both low and high speeds, the Short CB was found to be a consistent design for slamming reduction in comparison with the high CB.

Keywords: wave-piercing catamaran, hydroelastic segmented model, centre bow, relative motions, slamming, vertical bending moments

Introduction

Large wave piercing catamarans (WPCs) (Figure 1) are designed to provide high speed transportation above 35 knots mainly as vehicle/passenger ferries (Incat, 2018), but speed is often reduced in more severe seas. This paper investigates the motions and loads of a 112 m WPC at a reduced speed of 20 knots (i.e. Froude number = 0.32) by considering various centre bow (CB) and wet-deck configurations.

There are class restrictions requiring high speed passenger/vehicle ferries to reduce speed according to either wave height or slamming criteria to increase safety and passenger comfort (Faltinsen, 2006). Indeed, a medium speed operation mode considerably reduces motion amplitudes and global wave loadings, including slam-induced bending moments, compared to high speed operation (Lavroff and Davis, 2015; Lavroff et al., 2013; Shabani et al., 2017). Medium speed operation can also increase the transport energy efficiency (Davidson et al., 2011; Haase, 2015; Haase et al., 2016). However, ride control systems (a T-foil and stern

flaps) (Liang et al., 2016; Liang et al., 2018) are not effective at low to medium speeds and thus reduction in motions and loads may not be achieved (AlaviMehr et al., 2017a, b). There is therefore a need to investigate other means to minimise loads at medium speed, and in this regard the wet-deck height and centre bow length are key design parameters.

Severe slamming loads depend on interactions of the centre bow and incident waves (Davis et al., 2017; Thomas et al., 2003a; Thomas et al., 2003b). At full scale (Thomas, 2003) 96 m and an 86 m WPCs experienced a predominance of small slamming loads in the speed range between 10 and 15 knots. However, extreme, low probability slamming events can cause significant structural damage (Amin et al., 2013; Lavroff et al., 2013). Damage due to slamming includes distortion of the internal frames in the centre bow area and shell buckling (Amin, 2009; Thomas, 2003). Slamming can also lead to crack initiation and reduction of the fatigue life (Frangopol, 2016; Mondoro et al., 2016; Soliman et al., 2015; Thomas et al., 2008).

Early investigations using a hydroelastic segmented model (Lavroff et al., 2011; Matsubara et al., 2011; Thomas et al., 2011) of a 112 m WPC showed that the centre bow design (Figure 1) can affect both motion amplitude and the severity of slamming. Experimental tests and numerical simulations showed that the forward part of the centre bow, ahead of the intersection point (B) as shown in Figure 1, sprays the water freely in the lateral direction (McVicar et al., 2018; Shabani et al., 2017). Aft of this intersection point arch filling of the cross section increases slam severity (Shahraki et al., 2018; Swidan et al., 2016).

Design of an optimal centre bow and wet-deck geometry must consider the centre bow length and wet-deck height and their effect on slamming severity, hull bending and motions. Shabani et al. (2018 a, b, c) and Shahraki et al. (2018) found that centre bow length and archway clearance are key factors that contribute to the arch filling and slamming severity. The present paper extends the high speed investigation at 38 knots full scale (Shabani et al., 2018 a, b, c) of the effect of centre bow and wet-deck geometry on heave, pitch and CB loads and vertical bending moments to medium speed (20 knots). In addition, this paper provides a comparison of the maximum loads and motions in regular waves between the two speeds for various centre

bow and wet-deck configurations.

Experimental technique

Tank testing of a hydroelastic model with various centre bow configurations

A 2.5m hydroelastic segmented catamaran model (HSM02) shown in Figure 2(a), developed by (Rafie Shahraki, 2014), was used for tank testing in regular head seas. The forward, middle and aft segments of the model were connected by four aluminium links to produce a bending rigidity at model scale that represents the hydroelastic behaviour of the full scale vessel with a full scale first longitudinal mode of vibration (whipping frequency) of 2.2 Hz. The procedure to achieve this is illustrated in (Lavroff et al., 2011) with full investigations on scale model whipping frequencies in wet and dry modes. Figure 2(b) shows the locations of the elastic links at forward and aft cuts located at 56% and 33% of the model length from the transom respectively. Design details including the dimension of the elastic links, the model mass distribution and pitch radii of gyration of the segments are given by (Rafie Shahraki, 2014).

The tank tests included five centre bow and wet-deck configurations, designated here the “parent”,” high”, “low”, “long” and “short” centre bows (CB). Table 2 provides the dimensionless design parameters of all five configurations. Figure 3 compares the geometry of each alternate configuration with the parent CB.

The catamaran model was instrumented with a set of sensors as listed in Table 3 and the tests were conducted at the Australian Maritime College towing tank (100 m long, 3.5 m wide) according to the test conditions presented in Table 4. The water depth in the towing tank was set to 1.4 m.

Identification of external forces components

Measurements from two ATI load cells and two Brüel & Kjær accelerometers were used to identify the slam loads. The loads and moments acting on the CB segment are shown in Figure 4 where the CB segment is considered as a simplified two-dimensional rigid hull. $F_{\mathrm{z}}^{\mathrm{aft}}$, $F_{\mathrm{z}}^{\mathrm{fwd}}$ are vertical forces, $F_{\mathrm{x}}^{\mathrm{aft}}$,$F_{\mathrm{x}}^{\mathrm{fwd}}$ are longitudinal forces and $T_{\mathrm{y}}^{\mathrm{aft}}$, $T_{\mathrm{y}}^{\mathrm{fwd}}$ are moments measured by the aft and forward load cells. $\vec{R}$ shows an

external force vector and c_{cb} shows the centre of gravity of the centre bow segment. The dynamic equilibrium in the *x*-*z* plane of the CB segment at its centre of gravity gives

$$\begin{aligned} F_{\mathrm{x}}^{\mathrm{aft}} + F_{\mathrm{x}}^{\mathrm{fwd}} + R_x &= m_{cb}.a_x \\ F_{\mathrm{z}}^{\mathrm{aft}} + F_{\mathrm{z}}^{\mathrm{fwd}} + R_z &= m_{cb}.a_z \\ \sum M_c &= I_c.\alpha \end{aligned} \qquad (1)$$

where R_x and R_z are longitudinal and vertical components of the external force $\vec{R}$, a_x and a_z denote longitudinal and vertical CB accelerations respectively, α denotes CB angular acceleration, $\sum M_c$ denotes the nett moment acting at the CB centre of gravity, m_{cb} denotes the mass of CB segment and I_c represents mass moment of inertia about the *y*-axis which passes through the CB centre of gravity. Note that only the vertical and longitudinal component of external forces R_x and R_z will be presented here.

Results

Heave, pitch and vertical accelerations

Data was obtained from the stationary and moving wave probes to calculate measured wave amplitudes and wave encounter frequencies. LVDT data gave heave and pitch responses. Figure 5 shows sample time records of the heave and pitch for the parent bow configuration in 60 mm waves at a speed of 1.53 m/s. At $\omega_e^* = 2.34$, which represents encounters with long waves, the amplitudes of heave and pitch are large but they become much smaller at $\omega_{\mathrm{e}}^* = 5.3$, which represents encounter with short waves. Assuming sinusoidal motion, the dimensionless amplitudes of the heave and pitch accelerations are

$$\text{Dimensionless amplitude of the heave acceleration} = \frac{H_a\omega_e^2}{\left(\frac{\zeta_a g}{L_m}\right)} = \frac{H_a}{\zeta_a} \times \left(\omega_e\sqrt{\frac{L_m}{g}}\right)^2 = H^*\omega_e^{*2} \qquad (2)$$

$$\text{Dimensionless amplitude of the pitch acceleration} = \frac{\theta_a \omega_e^2}{\frac{2\pi\zeta_a}{\lambda}\left(\frac{g}{L_m}\right)} = \frac{\theta_a}{\frac{2\pi\zeta_a}{\lambda}} \times \left(\omega_e \sqrt{\frac{L_m}{g}}\right)^2$$

$$= \theta^* \omega_e^{*2} \tag{3}$$

where, H_a and θ_a are the amplitudes of the heave and pitch, ω_e is the angular wave encounter frequency, ζ_a is the wave amplitude, g is the gravitational acceleration, L_m is the overall model length, λ is the wavelength, $H^* = \frac{H_a}{\zeta_a}$ and $\theta^* = \frac{\theta_a}{\frac{2\pi\zeta_a}{\lambda}}$ denote dimensionless heave and pitch amplitudes respectively, and ω_e^* $= \omega_e \sqrt{\frac{L_m}{g}}$ is the dimensionless wave encounter frequency. It is noted that motions only differed significantly from sinusoidal motions at low amplitudes (e.g. heave in Figure 5(c)). It should also be noted that equations 2 and 3 are accelerations due to global motions excluding slamming acceleration.

Figures 6 and 7 show the effect of various CB configurations on dimensionless heave and pitch accelerations in 60, 90 and 120 mm waves as a function of dimensionless wave encounter frequency (ω_e^*) and wavelength ratio (λ/L_m) . The model with the high CB had the highest level of accelerations in heave and pitch for most encounter frequencies. The bow length had little effect on heave and pitch accelerations, with the short CB experiencing slightly greater heave accelerations, but slightly smaller pitch accelerations, compared to the parent CB in 60 and 90 mm waves.

Figure 8 compares the longitudinal distributions of vertical acceleration amplitudes at $\omega_e^* \cong 4.53$ for various CB configurations relative to the parent CB. It shows that increasing the wet-deck height can reduce passenger comfort significantly at all points but particularly forward of the LCG. However, changing the centre bow length only gives a small change in vertical motions. These design considerations can be more critical at high speeds (Shabani et al., 2018 b,c) as the differences between full speed and reduced speed for pitch and heave amplitudes are noticeable. Refer to Section 4 for more details.

Loads acting on the centre bow

Photographs of the model during slamming are shown in Figure 9. Figure 10 (a-c) shows time records of the vertical CB loads. Load and acceleration signals were filtered using a low pass digital filter with a cut off frequency 200 Hz. $R_z = -(F_z^{aft} + F_z^{fwd}) + m_{cb}.a_z$ represents the total CB vertical force (dashed line in Figure 10(c)). This force was disaggregated into two components (F_z^{slam} and F_z^{be}). The peak vertical slamming load (F_z^{slam}) is

$$F_z^{slam} = R_z^{peak} - F_z^{be}, \quad (4)$$

where, R_z^{peak} is the peak vertical force acting on the CB segment at a slam instant and F_z^{be} is the maximum bow entry force estimated by applying a low pass Butterworth filter on the force signal R_z with 5 Hz cut of frequency as presented in Figure 10 (c).

The peak vertical $\left(R_z{}^{peak}\right)$ and longitudinal $(R_x{}^{peak})$ CB loads acting on the CB segments prior to disaggregation are shown in Figures 11 and 12. The magnitudes of CB vertical loads increase as the wet-deck height decreases from the high CB to the parent CB for 60 mm, 90 mm and 120 mm waves (Figure 11(a-c)) but the difference in CB vertical loads between the low and parent CB is small. The CB vertical loads also increased significantly with increase of the CB length in both 60 mm and 90 mm (Figure 11(d & e)). The vertical CB loads ranged between 19% and 105% of the weight of the catamaran model (266 N) depending on centre bow configuration and wave height. The effect of wave height on CB vertical loads was significant. The parent CB showed an increase of about 67% in 90 mm waves and 133% in 120 mm waves compared to 60 mm waves.

The effect of the centre bow configuration on the longitudinal CB loads was not as significant as for the vertical CB loads. Figure 12 shows that longitudinal CB loads slightly increase as the bow length increases. In the case of the parent CB, the maximum longitudinal CB load was about 11% and 22% of the model weight in 60 mm and 90 waves respectively.

The maximum longitudinal CB loads were as low as 22% and as high as 33% of the vertical CB loads for loads obtained at 1.53 m/s. These ratios indicate that the directions of the resultant vector $\vec{R}$ of both

longitudinal and vertical components of CB loads had a vector direction in the range between 12º and 18º (anti-clockwise positive) with respect to the vertical plane. Although the maximum heave and pitch accelerations occurred in the range $\omega_e^* = 3.0 - 4.0$ (Figures 6&7) all maximum CB vertical loads occurred in the range $\omega_e^* = 4.0 - 5.0$, which corresponds to wavelength ratios (λ/L_m) between 1.15 and 0.85.

Figures 13 and 14 show vertical slamming loads (calculated using Equation 4) and bow entry loads respectively. The most severe slamming loads found in 90 mm and 120 mm ranged between 38% and 68% of the weight of catamaran model depending on the wet-deck height and CB configuration. The slamming loads of the high CB and short CB were considerably lower than the low, parent and long CBs. Therefore, at medium speed, hypothetically, the combination of the high and short CBs could provide the lowest slamming loads although this can be also one of the least preferred options when it comes to passenger comfort. Motions and loads in irregular waves, however, need to be investigated considering more authentic design options.

Vertical bending moments

Sample records of vertical bending moments measured at the forward cut of the catamaran model with parent CB and total vertical loads acting on the CB segment are shown in Figure 15 (a) and 15 (b) for $\omega_e^* = 4.52$ in 60 mm and 90 mm waves. The effect of centre bow length and wet-deck height on total (i.e. both hulls combined) sagging and hogging moments at the forward and aft cuts of the model in 60 and 90 mm waves is shown in Figures 16 and 17. As can be seen in Figure 16 both high and short CBs have smaller maximum sagging (but not hogging) moments than the parent CB in both 60 and 90 mm waves. The long CB also has slightly greater sagging moments compared to the parent CB.

The relationships between the magnitudes of total vertical loads acting on the centre bow and peak VBMs in both wave heights were investigated by collecting all CB load and VBM peak data obtained from various wave encounter frequencies. These data are presented in Figure 18 (a) and 18 (b) with linear regressions; the correlation factors and root mean square errors are summarised in Table 5. As can be seen, good correlation exists between the peak VBMs and total vertical loads in both 60 mm and 90 mm waves. In 90 mm waves,

both total vertical loads and peak VBMs showed approximately a two-fold increase compared to that in 60 mm waves. The linear models also suggest that the total vertical loads are not only greater in larger waves but also can occur at a greater distance to the forward cut when compared to smaller waves. This is also consistent with the locations of slamming pressures as shown by Shabani et al.(2019 a,b). Previous work by Davis et al. (2017) showed quite strong relationship between slam loads and VBMs in irregular waves for small and moderate strength slamming but not for strong slamming. This is not quite the case in regular waves as there is less scatter than that observed in irregular waves, and therefore, a regression model in regular waves should be considered with higher uncertainty as one can expect in realistic waves.

Comparison between reduced speed and full speed

In this section, the effect of speed for various centre bow and wet-deck configurations is presented by comparing the maximum values of the responses at 1.53 m/s to that previously (Shabani et al., 2018 b, c) obtained at 2.89 m/s (i.e. the design speed of 38 knots full scale). All data are summarised in Table 6.

When comparing the low speed and high speed results, it was found that the maxima of H^* at 1.53 m/s were reduced by a percentage in the range between 39% and 50% of that at 2.89 m/s, depending on the bow and wet-deck configuration and wave amplitude. Similarly, the maxima of P^* at 1.53 m/s were reduced by a percentage in the range between 14% and 32% of that at 2.89 m/s. Figure 19 shows these variations in 90 mm waves. Further analyses showed, with reference to the results presented in Figure 8, that the mean vertical accelerations at $\omega_e^* \cong 4.53$ along the hull, calculated over the length of passenger deck area which extends approximately from 5% to 70% of the overall length, were between 0.16 g and 0.21 g in 90 mm waves and between 0.1 g and 0.13 g in 60 mm waves, depending on the bow and wet-deck geometry, compared to the mean vertical accelerations calculated at 2.89 m/s.

Previous results also indicated that the parent CB experienced total vertical loads averaging 0.51 and 1.04 times the model weight in 60 mm and 90 mm waves respectively at a speed of 2.89 m/s (Shabani et al., 2018b). These compare to 0.44 and 0.78 times the model weight in the present tests at a speed of 1.53 m/s for 60 mm and 90 mm waves respectively (see Table 6 for other CBs). Thus, speed reduction gives a small

improvement in 60 mm waves (2.7 m waves at full scale) but the benefits become much more significant in large waves, whereby loads are reduced by 30% in 4 m waves (full scale) upon reducing speed from 38 to 20 knots. The effect of various CB and wet-deck configuration on maximum CB loads and vertical bending moments is also shown in Figure 20. A combination of the short CB and high CB could potentially result in reductions in both slamming load and vertical bending moment more significantly at the lower speed, but this may not be the case for either heave or pitch amplitude when comparing the results at both speeds. In addition, as shown, there is no significant difference in maximum VBM at high speed between the high CB and parent CB which does not support a change from the parent CB for loads as the hull girder must be designed according to extreme loads.

Conclusions

The effect of centre bow and wet-deck geometry on motions and loads of wave piercing catamarans was studied at a medium speed in regular waves. Table 7 shows a summary of findings.

Heave, pitch and vertical accelerations due to motions were found to increase with increased wet-deck height. In 90 mm and 120 mm (regular) waves at a dimensionless encounter frequency of $\omega_e^* = 4.52$, the high CB showed about 0.1 g increase in vertical acceleration amplitude at the LCG with respect to the parent CB and 0.05 g in 60 mm waves. The heave and pitch accelerations of the high CB were also greater than the parent CB. In contrast, the length of the centre bow had little effect on motions.

The centre bow entry loads and slamming loads together caused maximum total vertical loads ranging between 18% and 105 % of the weight of the catamaran depending on the centre bow configuration and wave height. Slamming loads and centre bow entry loads both decreased with increased wet-deck height. Maximum longitudinal CB loads were between 22% and 33% of the vertical load, showing the directions of the resultant vector $\vec{R}$ to be in the range between 12º and 19º (anti-clockwise positive) with respect to the vertical plane.

The sagging moments increased with an increase of length of the centre bow and decreased with an increase

of wet-deck height. A good correlation was found between the total vertical loads and the VBMs measured at the forward and aft cuts of the segmented model, indicating that simple regression models can be used for estimating the VBMs based on the total vertical force acting on the centre bow in regular waves but higher uncertainties should be considered for strong load cases. The results showed that the aft cut VBMs are slightly smaller than forward VBMs.

Centre bow design requires a compromise between the motions and loads according to the operational conditions. Since the high CB showed higher vertical acceleration and thus reduced passenger comfort, slamming reduction can best be achieved by decreasing the centre bow length ratio to that of the short CB (18% of overall length) at both speeds examined.

The effectiveness of speed reduction to reduce motions and loads for various centre bow and wet-deck configurations was established. Wet-deck slamming loads are reduced when operating at low to medium speeds but stronger loads are to be expected in more severe seas. Speed reduction will influence the optimal CB and wet-deck design based on regular waves. Whether an ideal CB and wet-deck design differs at reduced speed compared to full speed merits further investigations but systematic model tests in random waves by considering novel designs for centre bow and wet-deck configurations are recommended prior to further optimising the design in the future.

Acknowledgements

This work was undertaken in collaboration between the University of Tasmania, Revolution Design and International Catamarans Tasmania (INCAT) through the support of the Australian Research Council Linkage Grant number LP0883540. The work of Dr Jalal Rafie Shahraki in the development and production of the hydroelastic segmented model is also gratefully acknowledged.

Declaration of interest statement: None

References

AlaviMehr, J., Lavroff, J., Davis, M.R., Holloway, D.S., Thomas, G.A., 2017a. An experimental investigation of ride control algorithms for high-speed catamarans Part 1: Reduction of ship motions. Journal of Ship Research 61 (1), 35-49.

AlaviMehr, J., Lavroff, J., Davis, M.R., Holloway, D.S., Thomas, G.A., 2017b. An Experimental Investigation of Ride Control Algorithms for High-Speed Catamarans Part 2: Mitigation of Wave Impact Loads. Journal of Ship Research 61 (2), 51-63.

Amin, W., 2009. Non-linear unsteady wave loads on large high-speed wave piercing catamarans. PhD Thesis, University of Tasmania.

Amin, W., Davis, M., Thomas, G., Holloway, D., 2013. Analysis of wave slam induced hull vibrations using continuous wavelet transforms. Ocean Engineering 58, 154-166.

Davidson, G., Roberts, T., Friezer, S., Thomas, G., Bose, N., Davis, M., Verbeek, R., 2011. 130m Wave piercer catamaran: A new energy efficient multihull operating at critical speeds, RINA, Royal Institution of Naval Architects-International Conference: High Speed Marine Vessels-Papers, pp. 61-72.

Davis, M.R., French, B.J., Thomas, G.A., 2017. Wave slam on wave piercing catamarans in random head seas. Ocean Engineering 135, 84-97.

Faltinsen, O.M., 2006. Hydrodynamics of high-speed marine vehicles. Cambridge university press, United Kingdom.

Frangopol, D.M., 2016. Integrating SHM and Time Variant System Performance of Naval Ship Structures For Near Real Time Decision Making Under Uncertainty: A Comprehensive Framework. Lehigh University Bethlehem United States.

Haase, M., 2015. Energy-Efficient Large Medium-Speed Catamarans: Hull Form Design by Full-Scale CFD. PhD Thesis. University of Tasmania.

Haase, M., Zurcher, K., Davidson, G., Binns, J.R., Thomas, G., Bose, N., 2016. Novel CFD-based full-scale resistance prediction for large medium-speed catamarans. Ocean Engineering 111, 198-208.

Incat, 2018.

Lavroff, J., Davis, M.R., 2015. Slamming kinematics, impulse and energy transfer for wave-piercing catamarans. Journal of Ship Research 59 (3), 145-161.

Lavroff, J., Davis, M.R., Holloway, D.S., Thomas, G., 2011. Determination of wave slamming loads on high-speed catamarans by hydroelastic segmented model experiments. International Journal of Maritime Engineering 153 (A3), 185-197.

Lavroff, J., Davis, M.R., Holloway, D.S., Thomas, G., 2013. Wave slamming loads on wave-piercer catamarans operating at high-speed determined by hydro-elastic segmented model experiments. Marine Structures 33, 120-142.

Liang, L., Yuan, J., Zhang, S., 2016. Application of model predictive control technique for wave piercing catamarans ride control system, Mechatronics and Automation (ICMA), 2016 IEEE International Conference on. IEEE, pp. 726-731.

Liang, L., Yuan, J., Zhang, S., Zhao, P., 2018. Design a software real-time operation platform for wave piercing catamarans motion control using linear quadratic regulator based genetic algorithm. PloS one 13 (4), e0196107.

Matsubara, S., Thomas, G., Davis, M.R., Holloway, D.S., Roberts, T., 2011. Influence of centrebow on motions and loads of high-speed catamarans, in: Peltzer, T.J. (Ed.), 11th International Conference on Fast Sea Transportation (FAST 2011). American Society of Naval Engineers, Honolulu, Hawaii, pp. 661-668.

McVicar, J., Lavroff, J., Davis, M.R., Thomas, G., 2018. Fluid–structure interaction simulation of slam-induced bending in large high-speed wave-piercing catamarans. Journal of Fluids and Structures 82, 35-58.

Mondoro, A., Soliman, M., Frangopol, D.M., 2016. Prediction of structural response of naval vessels based on available structural health monitoring data. Ocean Engineering 125, 295-307.

Rafie Shahraki, J., 2014. The influence of hull form on the slamming behaviour of large high speed catamarans. PhD Thesis, University of Tasmania.

Shabani, B., Holloway, D., Lavroff, J., Davis, M., Thomas, G., 2017. Systematic model tests on centre bow design for motion and slamming load alleviation in high speed catamarans, 14th International Conference on Fast Sea Transportation, pp. 136-143.

Shabani, B., Lavroff, J., Davis, M.R., Holloway, D.S., Thomas, G.A., 2018a. Slam loads and kinematics of wave-piercing catamarans during bow entry events in head seas. Journal of Ship Research 62 (3), 134-155.

Shabani, B., Lavroff, J., Holloway, D.S., Davis, M.R., Thomas, G.A., 2018b. The effect of centre bow and wet-deck geometry on wet-deck slamming loads and vertical bending moments of wave-piercing catamarans. Ocean Engineering 169, 401-417.

Shabani, B., Lavroff, J., Holloway, D.S., Davis, M.R., Thomas, G.A., 2018c. The influence of the centre bow and wet-deck geometry on motions of wave-piercing catamarans. Proceedings of the Institution of Mechanical Engineers, Part M: Journal of Engineering for the Maritime Environment, 1475090217753761.

Shabani, B., Lavroff, J., Davis, M.R., Holloway, D.S., Thomas, G.A., 2019a. Slam loads and pressures acting on high-speed wave-piercing catamarans in regular waves. Marine Structures 66: 136-153.

Shabani, B., Lavroff, J., Holloway, D.S., Davis, M.R., Thomas, G.A., 2019b. Wet-deck slamming loads and pressures acting on wave piercing catamarans." International Shipbuilding Progress 66 (3), 201-231.

Shahraki, J., Thomas, G., Davis, M., 2018. The Influence of Centre Bow Length On Slamming Loads and Motions of Large Wave-piercing Catamarans. Transactions of the Royal Institution of Naval Architects Part A: International Journal of Maritime Engineering.

Soliman, M., Barone, G., Frangopol, D.M., 2015. Fatigue reliability and service life prediction of aluminum naval ship details based on monitoring data. Structural Health Monitoring 14 (1), 3-19.

Swidan, A., Thomas, G., Ranmuthugala, D., Amin, W., Penesis, I., Allen, T., Battley, M., 2016. Experimental drop test investigation into wetdeck slamming loads on a generic catamaran hullform. Ocean Engineering 117, 143-153.

Thomas, G., Davis, M., Holloway, D., Roberts, T., 2008. The vibratory damping of large high-speed catamarans. Marine Structures 21 (1), 1-22.

Thomas, G., Davis, M., Holloway, D., Watson, N., Roberts, T., 2003a. Slamming response of a large high-speed wave-piercer catamaran. Marine Technology 40 (2), 126-140.

Thomas, G., Winkler, S., Davis, M., Holloway, D., Matsubara, S., Lavroff, J., French, B., 2011. Slam events of high-speed catamarans in irregular waves. Journal of Marine Science and Technology 16 (1), 8-21.

Thomas, G.A., Davis, M.R., Holloway, D.S., 2003b. The whipping vibration of large high speed catamarans. International Journal of Maritime Technology 145, 289-304.

Thomas, G.G.A., 2003. Wave slam response of large high-speed catamarans. PhD Thesis, University of Tasmania.

Table 1 Principal particulars of the HSM02 model and the 112 m Incat catamaran

	Catamaran Model (HSM02)	Full scale 112m Incat Catamaran
Overall length	2.5 m	112.6 m
Length (waterline)	2.36 m	105.6 m
Displacement	27.12 kg	2500 tonnes
Overall beam	0.68 m	30.5 m
Beam of demihulls	0.13 m	5.8 m
LCG (from transom)	0.941 m	42.15 m
Pitch radius of gyration (about LCG)	0.69 m	30.91 m

Table 2 Dimensionless design parameters for various Centre Bow (CB) and wet-deck configurations

	Dimensionless tunnel height (T_h/L) ×100 *	Dimensionless tunnel clearance (T_{cl}/L) ×100 **	Dimensionless centre bow length (L_{cb}/L) ×100 ***
High CB	7.1	3.8	24.3
Parent CB	6.0	2.7	24.3
Low CB	5.4	2.1	24.3
Long CB	6.0	2.7	30.3
Short CB	6.0	2.7	18.3

*Dimensionless tunnel height ($\boldsymbol{T_h/L}$) is the vertical distance between the flat wet-deck and the vessel's base line, $\boldsymbol{T_h}$, expressed as a ratio to the overall length, ($\boldsymbol{L}$). **Dimensionless tunnel clearance ($\boldsymbol{T_{cl}/L}$) is the vertical distance between the flat wet-deck and the design waterline (Figure 3a), $\boldsymbol{T_{cl}}$, expressed as a ratio to the overall length $\boldsymbol{L}$ *** Dimensionless centre bow length ($\boldsymbol{L_{cb}/L}$) is the longitudinal distance between the bow tip and centre bow truncated section, $\boldsymbol{L_{cb}}$, expressed as a ratio to the overall length ($\boldsymbol{L}$).

Table 3 Instrumentation used in model tests

Item	Quantity	Description of location	Description/Type
Load cell	2	Attached on the (i) forward and (ii) aft transverse beams*	Mini 45 ATI transducers
LVDT	2	(i) Aft and (ii) middle segments*	Linear Variable Differential Transformers
Static WP	1	9 m in front of the tank wave maker	Resistive type wave probe
Moving WP	2	Installed below the carriage at the (i) LCG and (ii) 1940 mm from the transom	Resistive type wave probes
Strain gauge	4 pairs	Model segment cuts at (i) aft starboard, (ii) forward starboard, (iii) aft port (iv) forward port*	350 Ohm , CEA series Vishay Micro Measurement
Accelerometer	2	Centre line of the CB segment at a separation distance of 550 mm*	Brüel & Kjær - Type 4370 & 4371 (1-axis) or Triaxial Brüel & Kjær**
Data Acquisition	1	Desktop computer located on towing tank carriage	National Instruments- M series NI6255

*Refer to Figure 2(b) for more details ** Type 4371 (1-axis) accelerometer was only used for the high and low CBs. It was replaced with a triaxial Brüel & Kjær charge accelerometer for the parent, long and short CBs.

Table 4 Model test conditions for HSM02 model tests with various centre bow and wet-deck configurations in regular waves at medium speed

	Model scale		Full-scale	
	Velocity	Wave height	Velocity	Wave height
	V_m (m/s)	h_w (mm)	V_s (knots)	H (m)
Condition 1*	1.53	60	20	2.7
Condition 2*	1.53	90	20	4.0
Condition 3**	1.53	120	20	5.4

*All configurations including the parent, high, low, short and long CBs were tested in various wave frequencies. ** Only the parent and high CBs were tested.

Table 5 Correlation factors, linear fits and goodness of the linear fits between the total vertical loads and peak VBMs at Fwd cut for the parent CB

	Nominal wave height	Fwd cut location from the model's transom	R-square	Linear fit $VBM(\text{Fwd}) = a1.R_z^{\text{peak}} + a2)$		RMSE of the linear fit
				$a1$(m)	$a2$ (N.m)	(N.m)
Figure 18 (a)	60 mm	1.4 m	0.77	0.19	8.55	2.34
Figure 18 (b)	90 mm	1.4 m	0.91	0.30	3.77	4.99

Table 6 Summary of average maximum values in RAOs for dimensionless heave, $\boldsymbol{H^*}$, pitch, $\boldsymbol{P^*}$, dimensionless vertical slam force, $\boldsymbol{F_z^{slam}/mg}$, and dimensionless vertical bending moments, $\boldsymbol{VBM/mgL}$, for various centre bow and wet-deck geometries at two speeds and waves heights

Speed	RAO	Wave Height	Parent CB	High CB	Low CB	Long CB	Short CB
1.53 m/s (Fn=0.32)	H^*	60 mm	1.05E+01	1.35E+01	1.03E+01	1.08E+01	1.20E+01
		90 mm	9.98E+00	1.20E+01	9.52E+00	1.04E+01	1.08E+01
	P^*	60 mm	1.34E+01	1.72E+01	1.44E+01	1.41E+01	1.37E+01
		90 mm	1.19E+01	1.46E+01	1.19E+01	1.27E+01	1.20E+01
	F_z^{slam}/mg	60 mm	4.45E-01	1.66E-01	4.42E-01	5.52E-01	2.74E-01
		90 mm	7.80E-01	5.78E-01	7.55E-01	9.20E-01	5.26E-01
	VBM/mgL	60 mm	5.15E-02	3.34E-02	6.10E-02	5.49E-02	4.27E-02
		90 mm	9.83E-02	8.93E-02	1.12E-01	1.07E-01	8.69E-02
2.89 m/s (Fn=0.60)	H^*	60 mm	2.11E+01	2.59E+01	1.95E+01	2.05E+01	2.15E+01
		90 mm	1.80E+01	2.20E+01	1.68E+01	1.86E+01	1.76E+01
	P^*	60 mm	1.97E+01	2.01E+01	1.92E+01	2.02E+01	1.85E+01
		90 mm	1.70E+01	1.77E+01	1.70E+01	1.82E+01	1.61E+01
	F_z^{slam}/mg	60 mm	5.09E-01	4.12E-01	5.83E-01	8.31E-01	3.71E-01
		90 mm	1.04E+00	1.01E+00	1.05E+00	1.40E+00	7.19E-01
	VBM/mgL	60 mm	5.38E-02	4.73E-02	6.92E-02	6.92E-02	4.19E-02
		90 mm	1.16E-01	1.17E-01	1.22E-01	1.31E-01	9.73E-02

Note that mg is the weight and L is the overall length of catamaran model, and VBM is the forward cut bending moment.

Table 7 Summary of findings

(1) Heave, pitch and vertical accelerations due to motions were found to increase with increased wet-deck height. In contrast, the length of the centre bow had little effect on motions.
(2) Slamming loads and centre bow entry loads both decreased with increased wet-deck height.
(3) The sagging moments increased with increased centre bow length and decreased with increased wet-deck height.
(4) Slamming reduction can best be achieved by decreasing the centre bow length ratio to that of the short CB (18% of overall length).
(5) Wet-deck slamming loads are reduced when operating at low to medium speeds but stronger loads are to be expected in more severe seas.

Figure 1

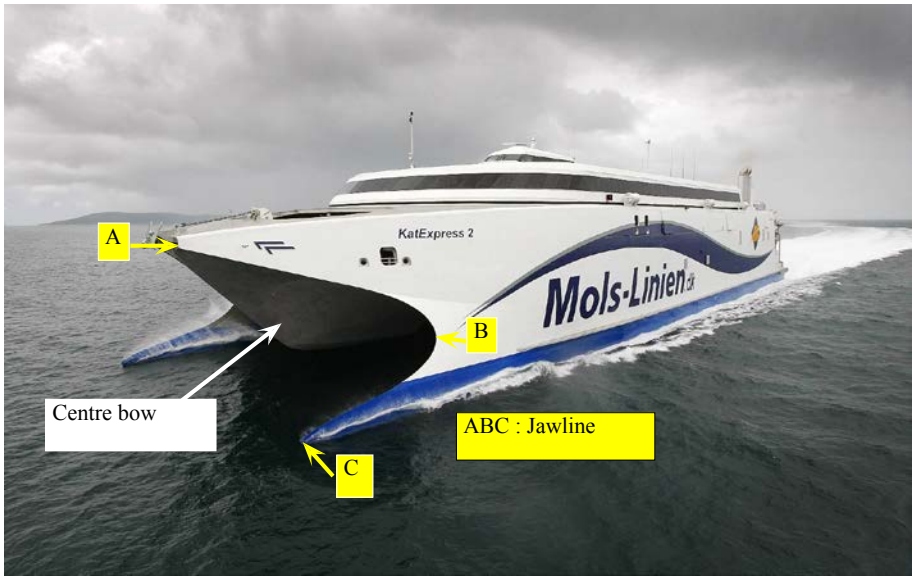

(a)

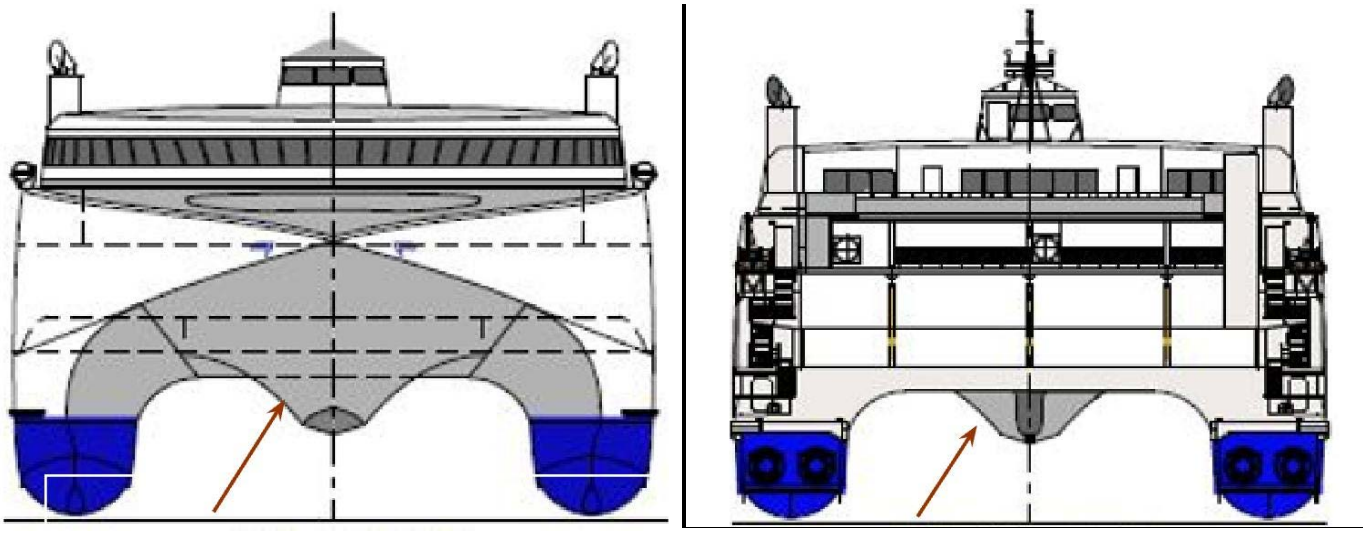

Centre bow (forward view)

Centre bow truncation (aft view)

(b)

Figure 2

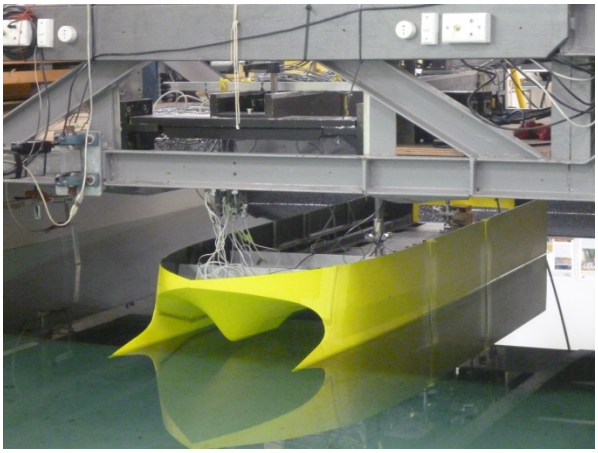

(a)

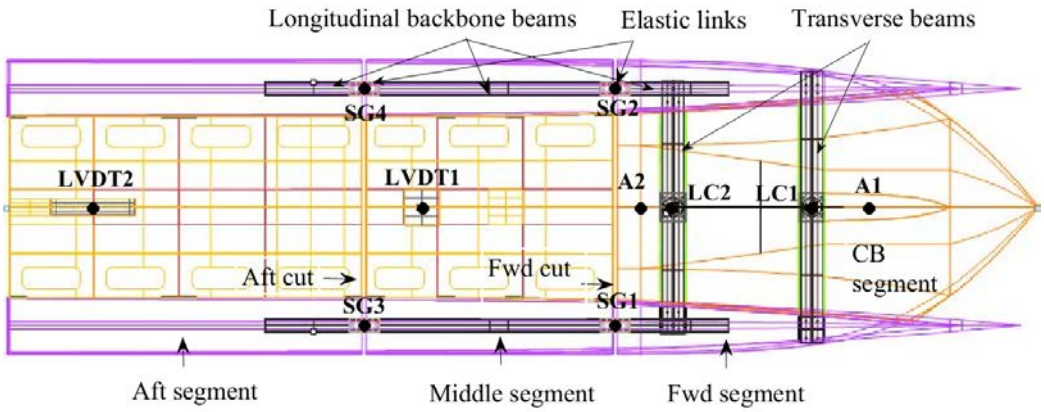
Longitudinal backbone beams
Elastic links
Transverse beams
SG4
SG2
LVDT2
LVDT1
A2
LC2
LC1
A1
CB
segment
Aft cut
Fwd cut
SG3
SG1
Aft segment
Middle segment
Fwd segment

(b)

Figure 3

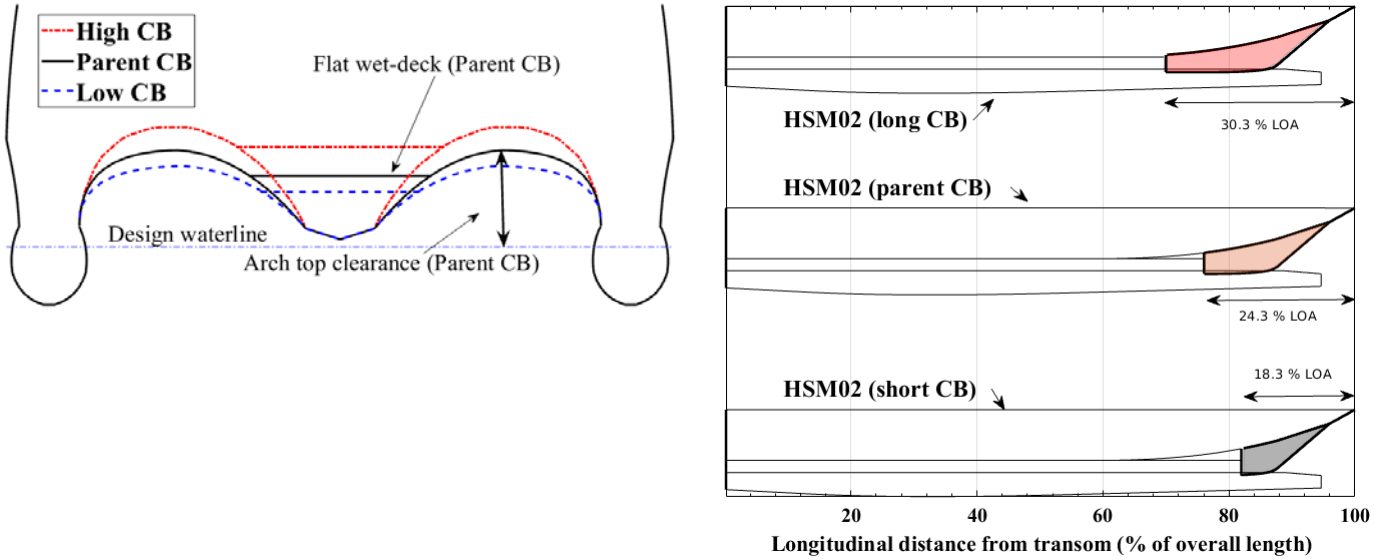
High CB
Parent CB
Low CB
Flat wet-deck (Parent CB)
Design waterline
Arch top clearance (Parent CB)
HSM02 (long CB)
30.3 % LOA
HSM02 (parent CB)
24.3 % LOA
18.3 % LOA
HSM02 (short CB)
20
40
60
80
100
Longitudinal distance from transom (% of overall length)

(a) (b)

Figure 4

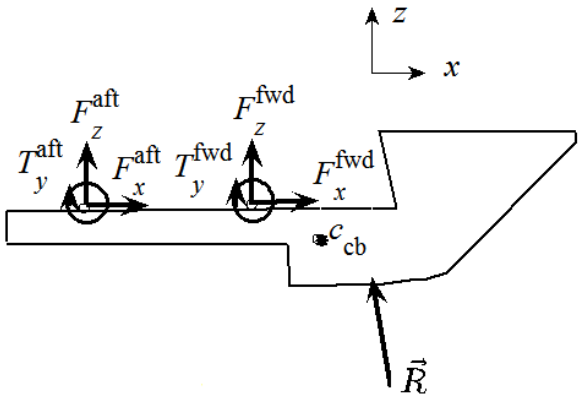

Figure 5

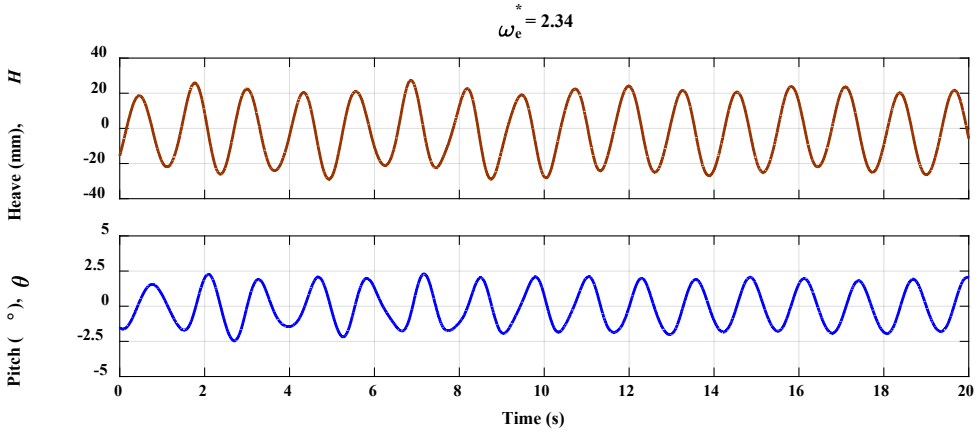
$\omega_e^* = 2.34$
Heave (mm), H
Pitch (°), θ
Time (s)

(a)

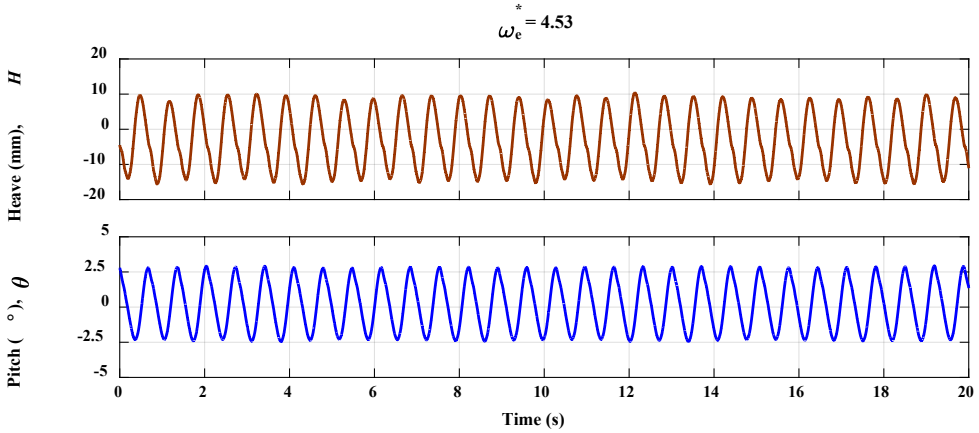
$\omega_e^* = 4.53$
Heave (mm), H
Pitch (°), θ
Time (s)

(b)

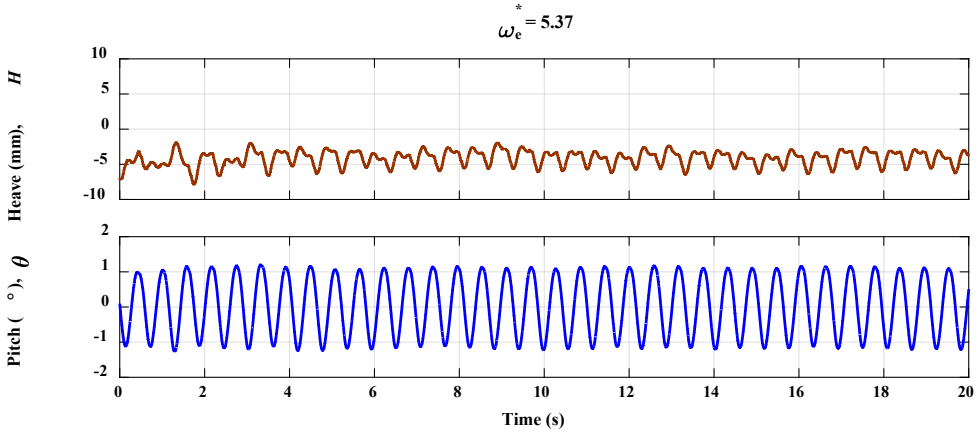
$\omega_e^* = 5.37$
Heave (mm), H
Pitch (°), θ
Time (s)

(c)

Figure 6

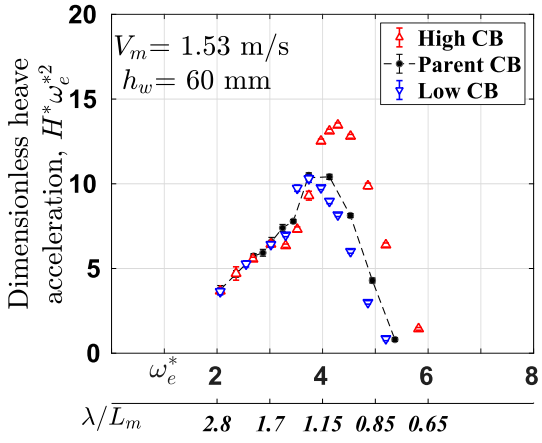

(a)

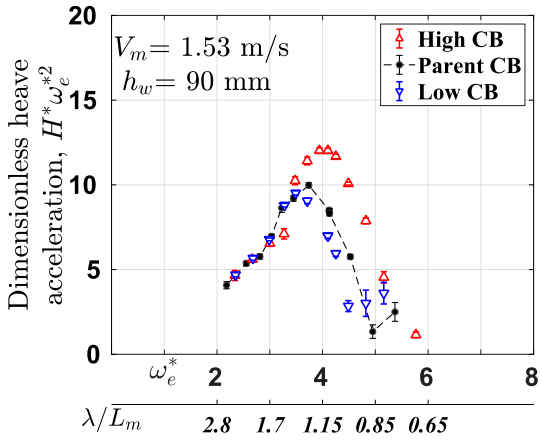

(b)

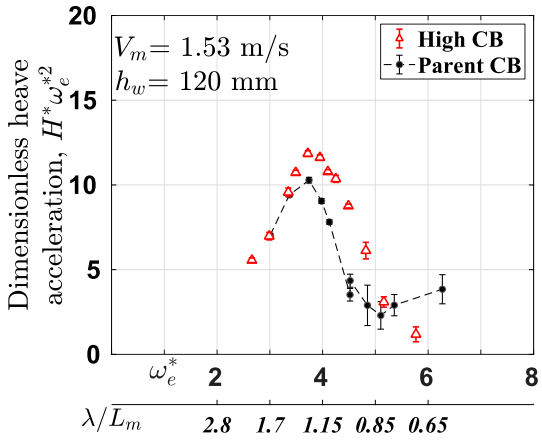

(c)

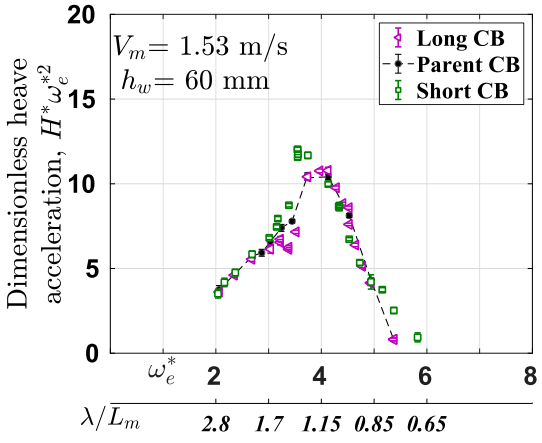

(d)

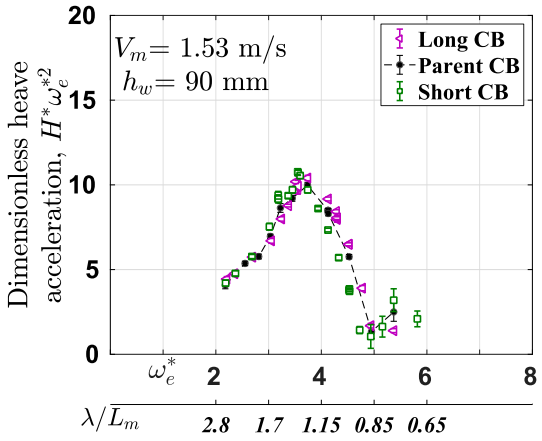

(e)

Figure 7

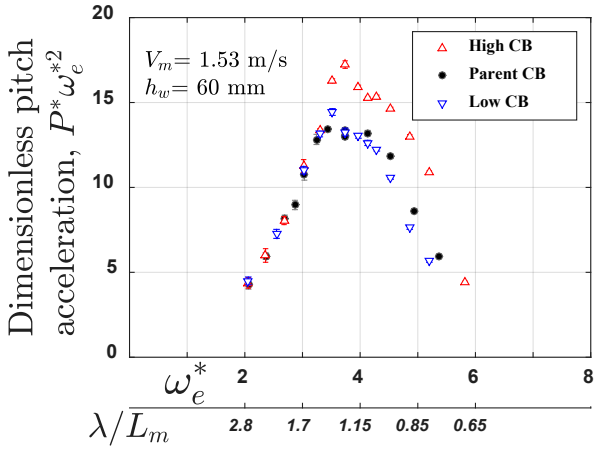

(a)

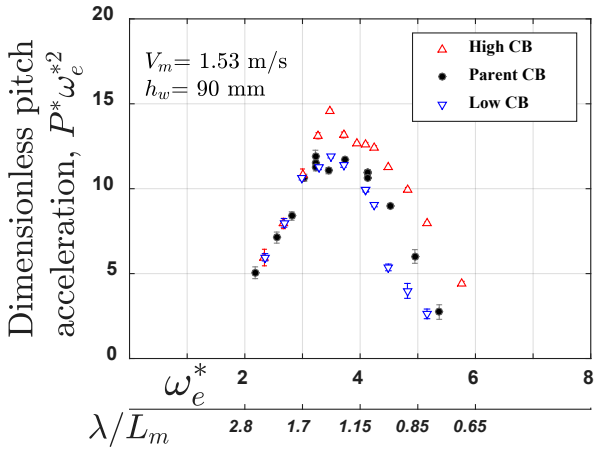

(b)

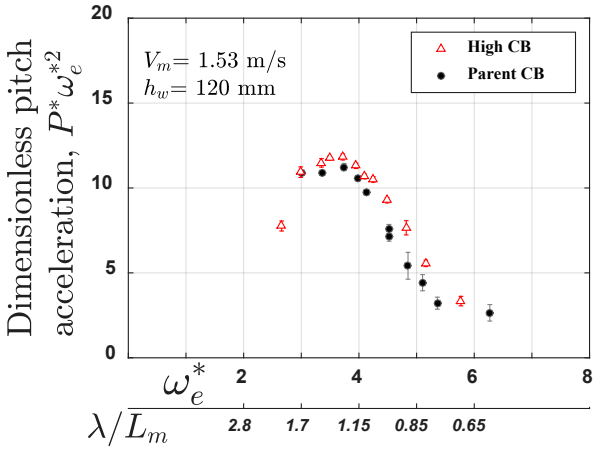

(c)

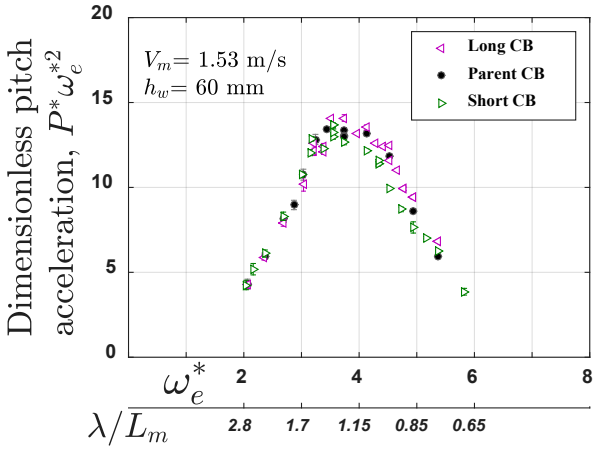

(d)

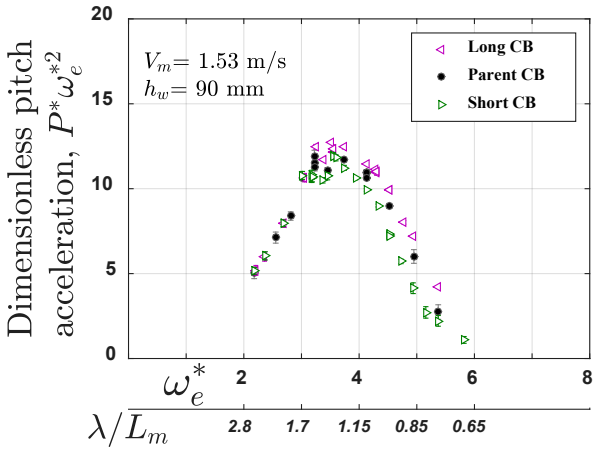

(e)

Figure 8

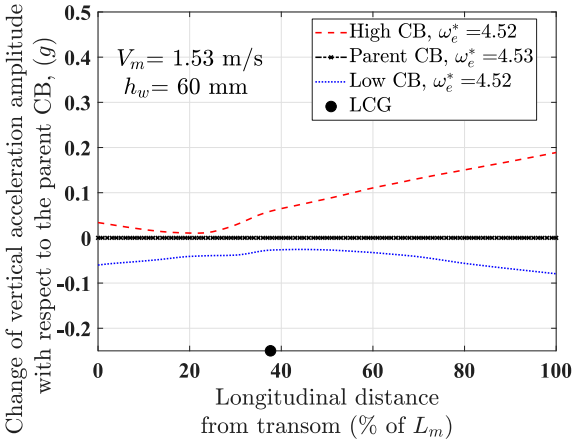

(a)

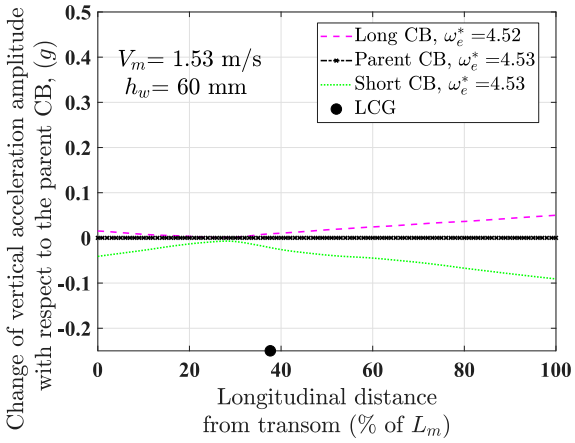

(d)

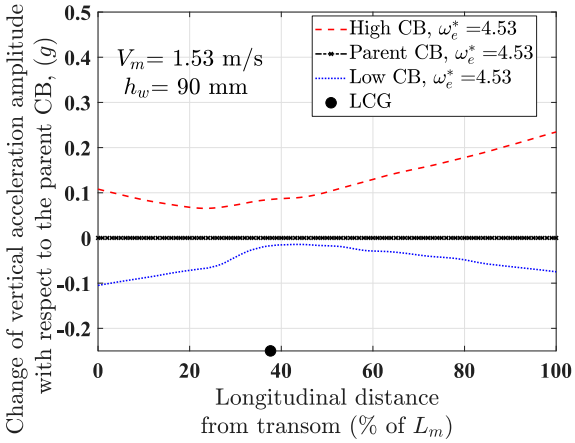

(b)

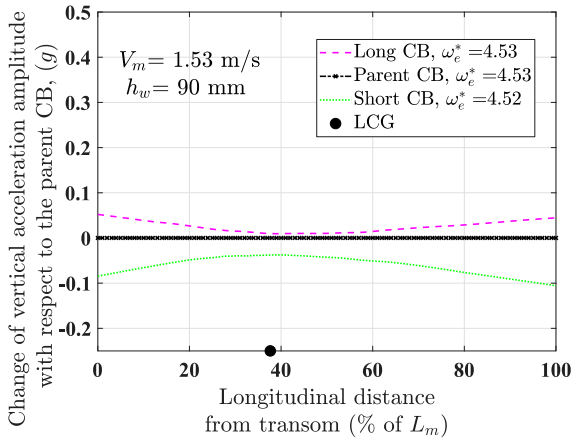

(e)

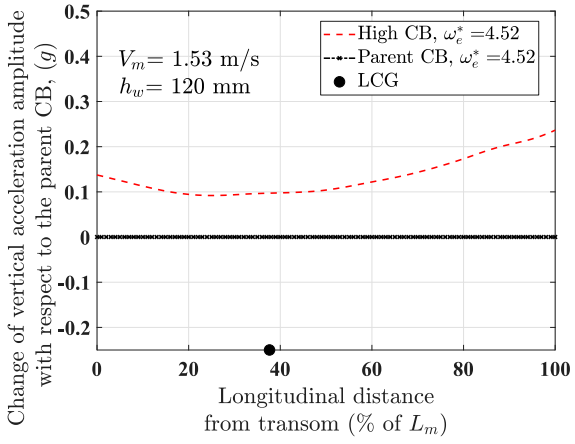

(c)

Figure 9

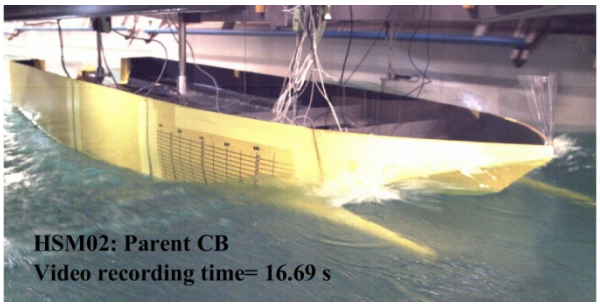
HSM02: Parent CB
Video recording time= 16.69 s

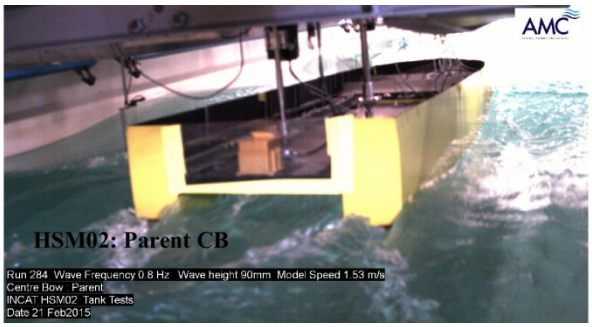
AMC
HSM02: Parent CB
Run 284 Wave Frequency 0.8 Hz Wave height 90mm Model Speed 1.53 m/s
Centre Bow Parent
INCAT HSM02 Tank Tests
Date 21 Feb2015

Figure 10

(a)

(b)

(c)

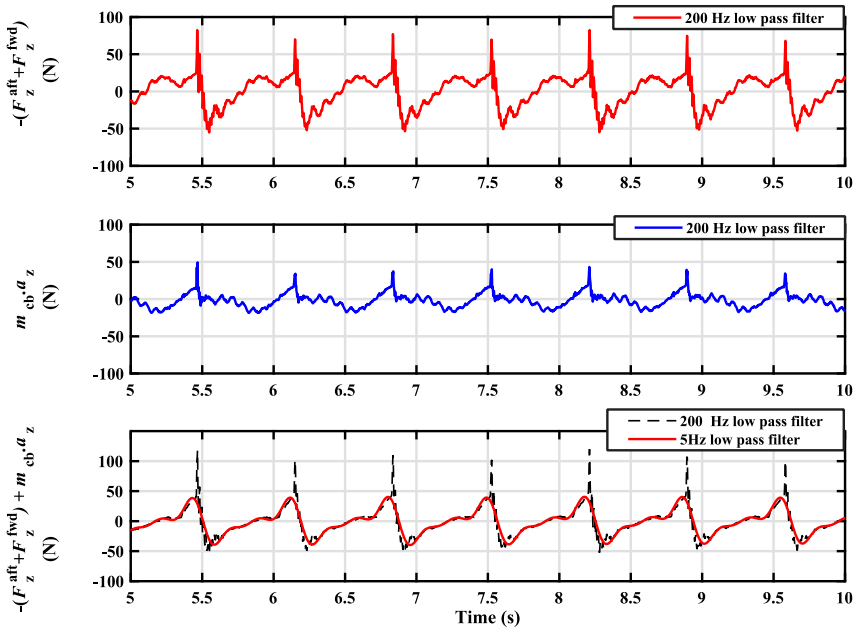

Figure 11

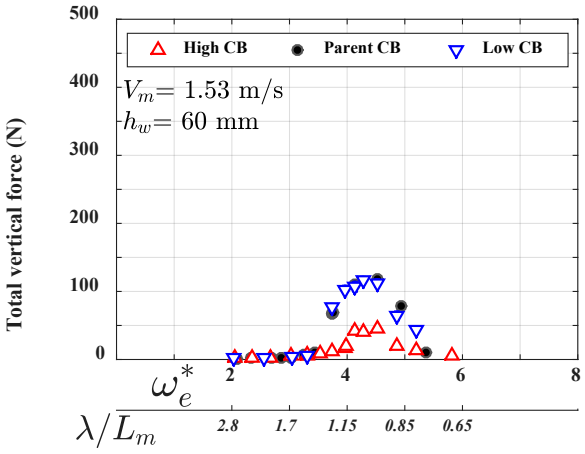

(a)

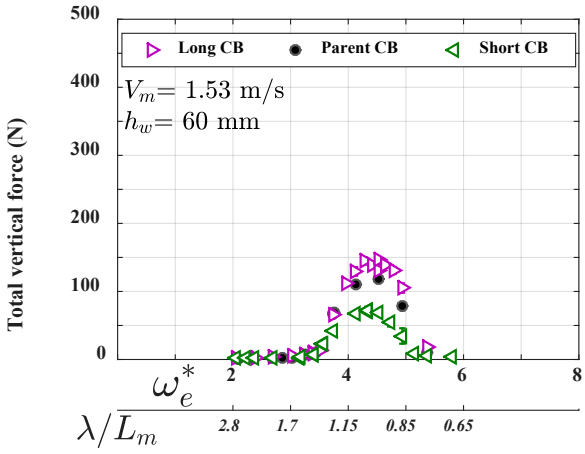

(d)

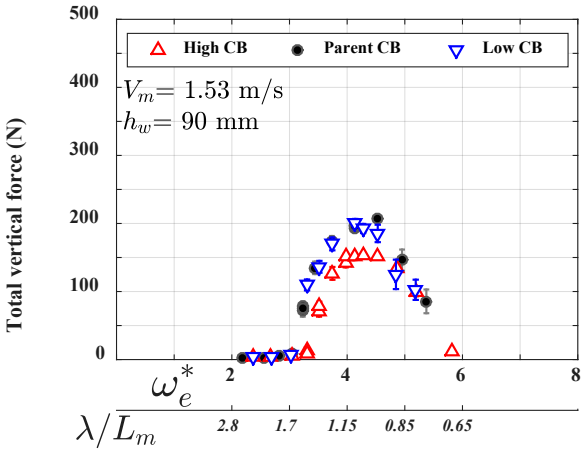

(b)

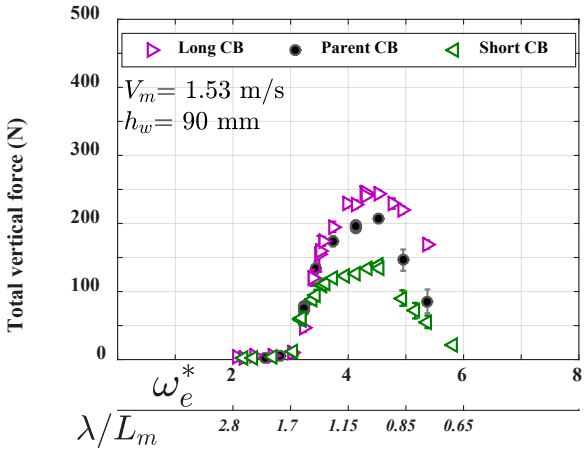

(e)

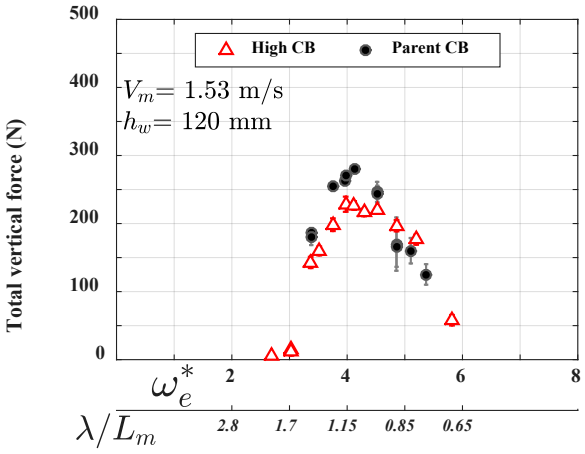

(c)

Figure 12

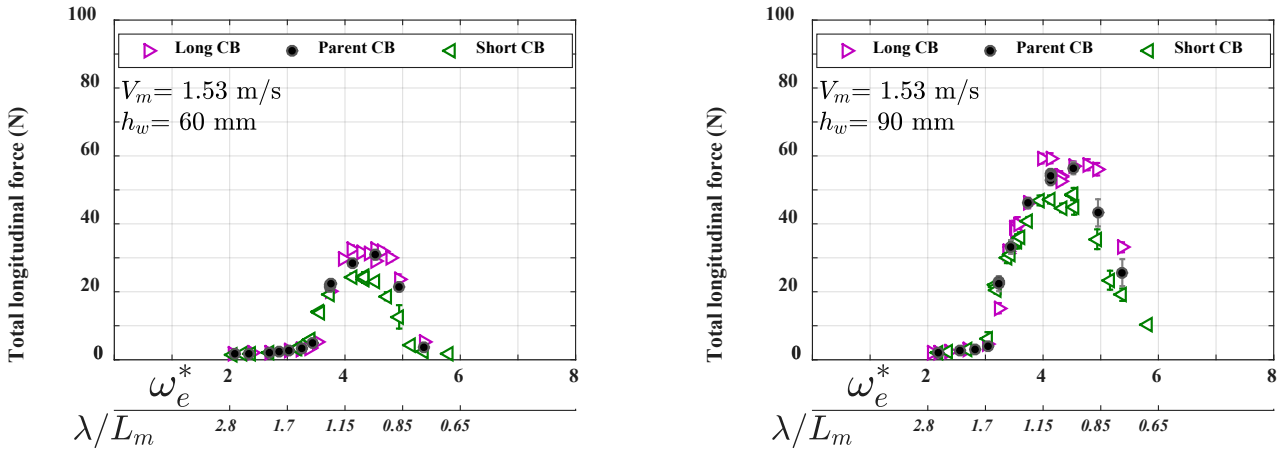
Long CB
Parent CB
Short CB
V_m= 1.53 m/s
h_w= 60 mm
Total longitudinal force (N)
100
80
60
40
20
0
2
4
6
8
ω_e^*
λ/L_m
2.8
1.7
1.15
0.85
0.65
Long CB
Parent CB
Short CB
V_m= 1.53 m/s
h_w= 90 mm
Total longitudinal force (N)

(a) (b)

Figure 13

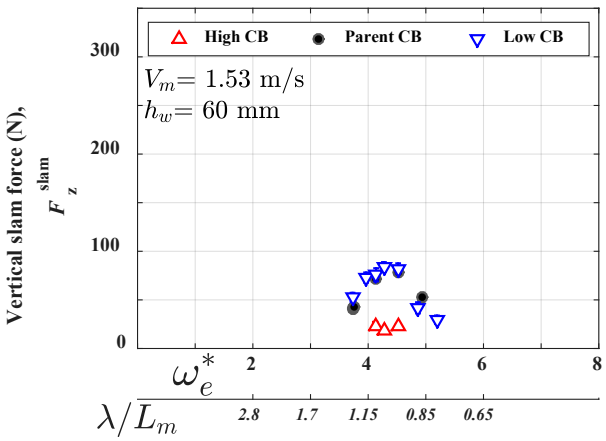

(a)

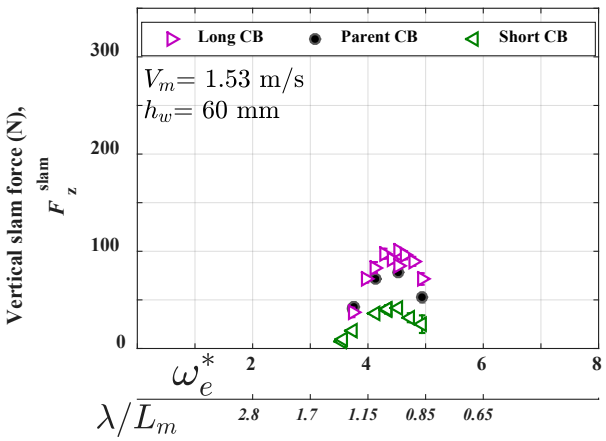

(b)

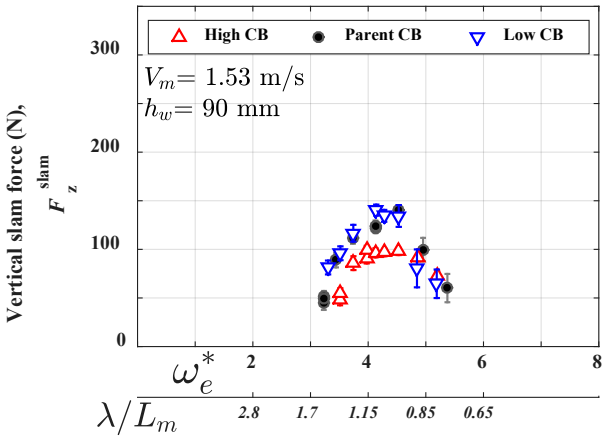

(c)

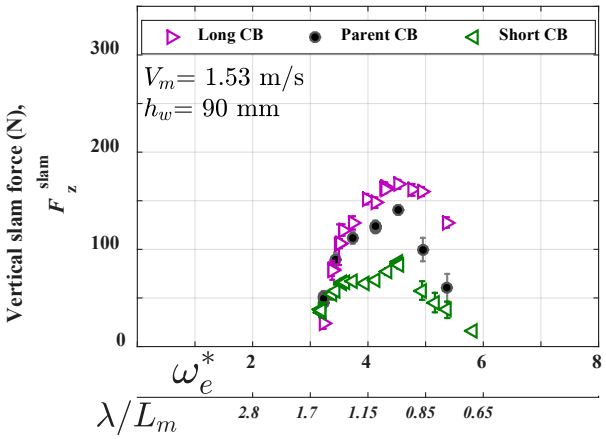

(d)

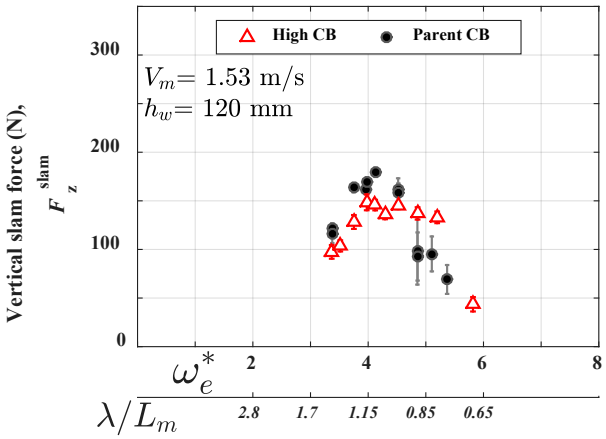

(e)

Figure 14

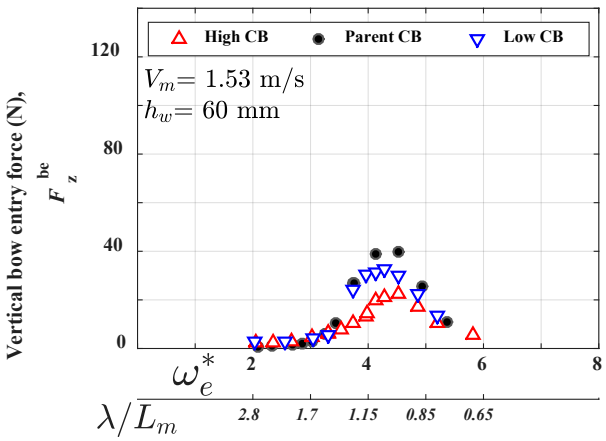

(a)

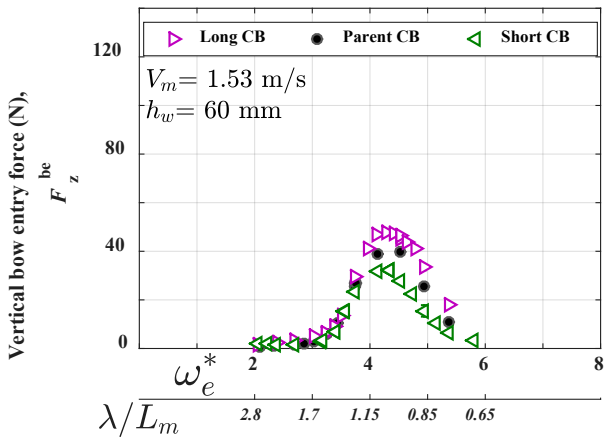

(e)

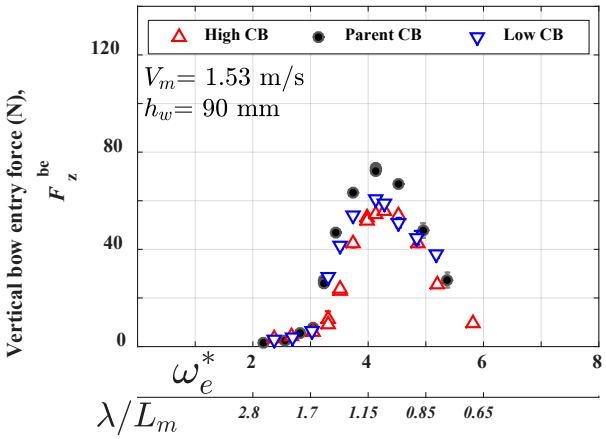

(b)

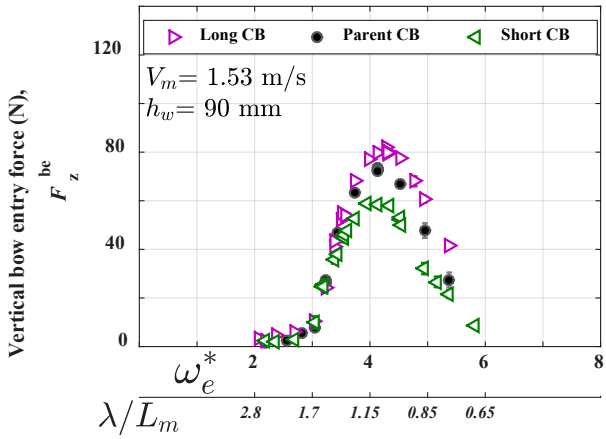

(f)

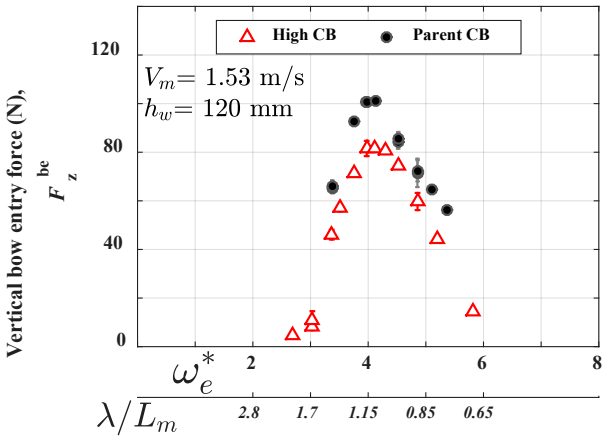

(c)

Figure 15

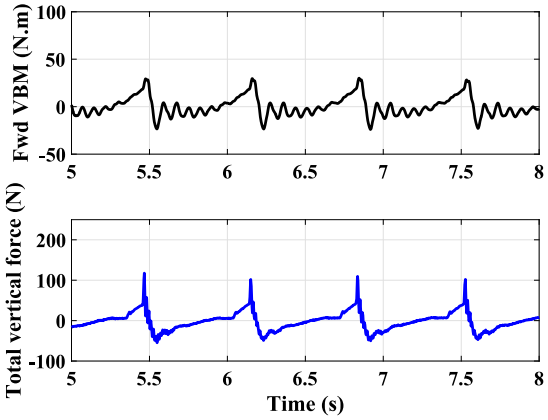
Fwd VBM (N.m)
100
50
0
-50
5
5.5
6
6.5
7
7.5
8
Total vertical force (N)
200
100
0
-100
Time (s)

(a)

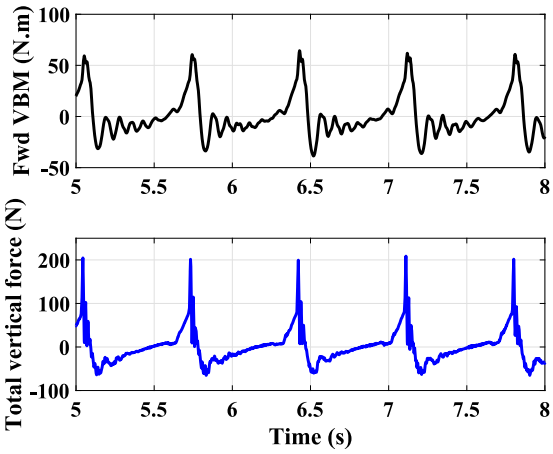
Fwd VBM (N.m)
100
50
0
-50
5
5.5
6
6.5
7
7.5
8
Total vertical force (N)
200
100
0
-100
Time (s)

(b)

Figure 16

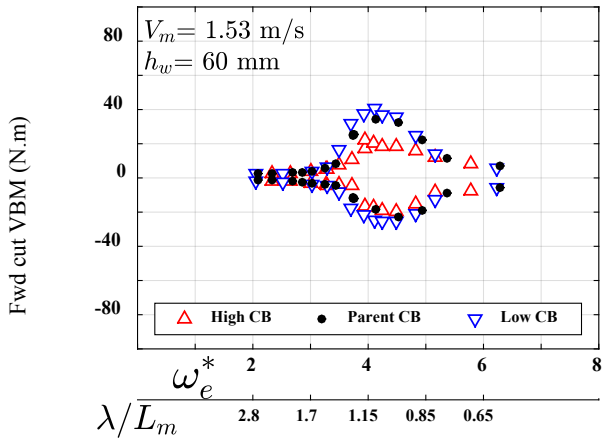

(a)

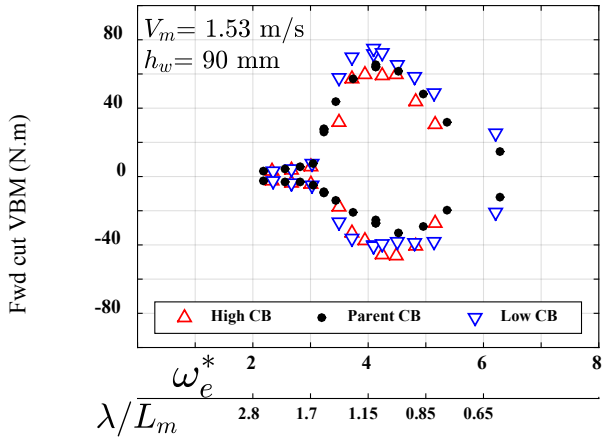

(b)

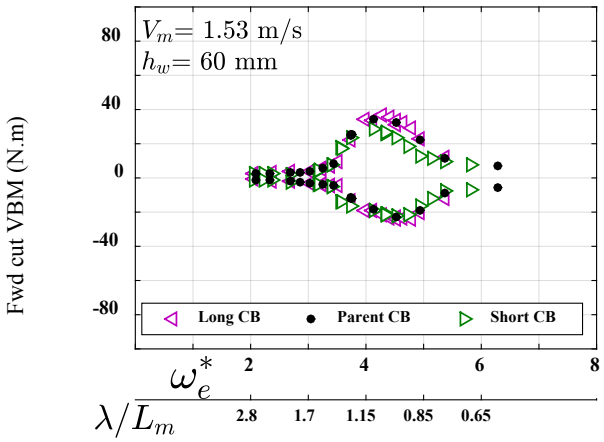

(c)

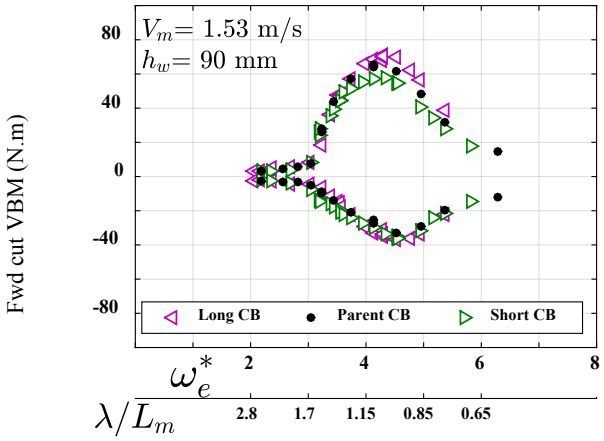

(d)

Figure 17

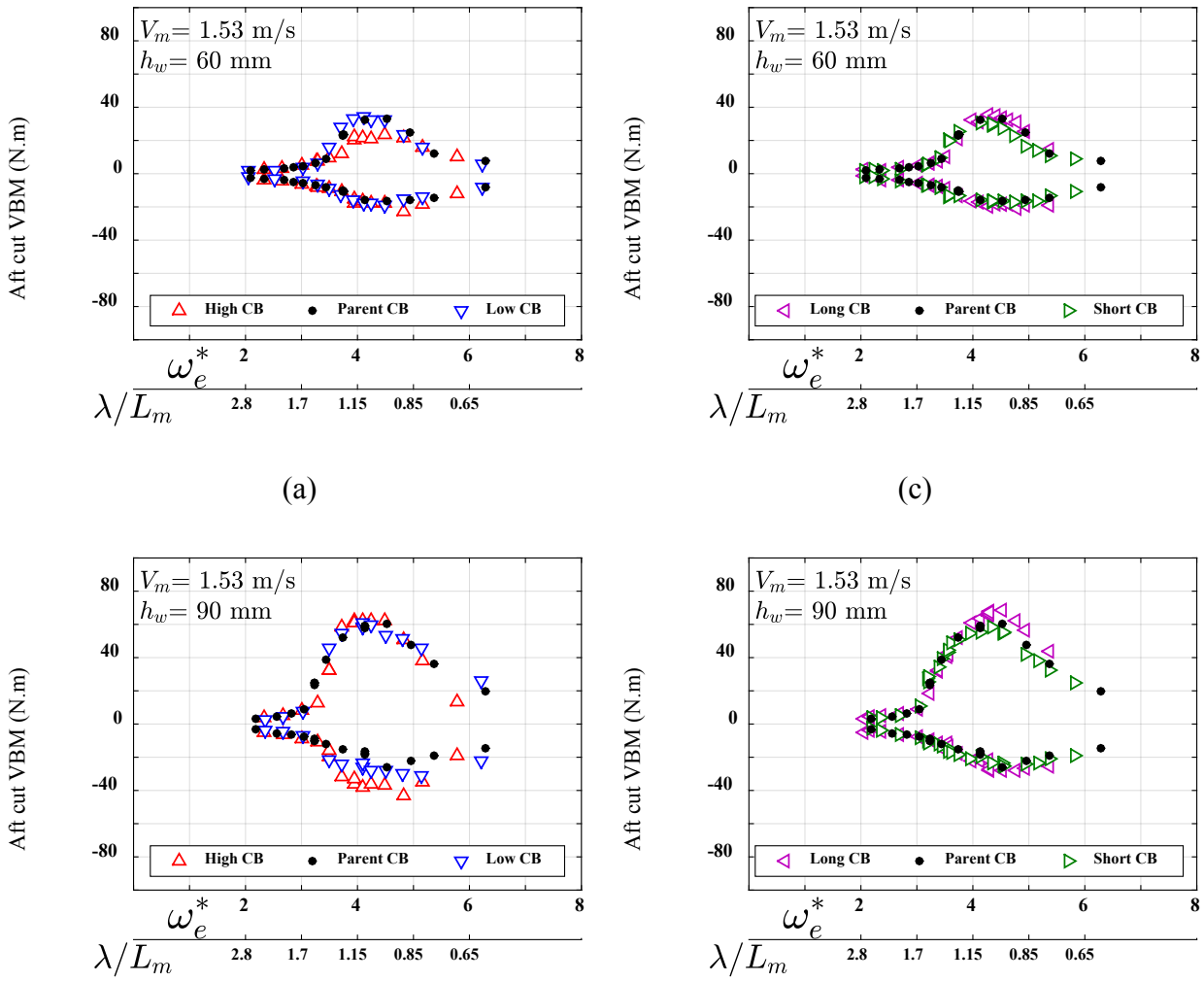
V_m= 1.53 m/s
h_w= 60 mm
Aft cut VBM (N.m)
80
40
0
-40
-80
High CB
Parent CB
Low CB
ω_e^*
2
4
6
8
λ/L_m
2.8
1.7
1.15
0.85
0.65
(a)
V_m= 1.53 m/s
h_w= 60 mm
Aft cut VBM (N.m)
Long CB
Parent CB
Short CB
(c)
V_m= 1.53 m/s
h_w= 90 mm
Aft cut VBM (N.m)
High CB
Parent CB
Low CB
(b)
V_m= 1.53 m/s
h_w= 90 mm
Aft cut VBM (N.m)
Long CB
Parent CB
Short CB
(d)

Figure 18

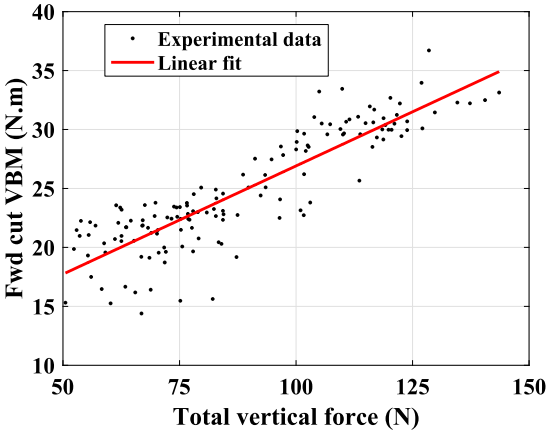
Experimental data
Linear fit
Fwd cut VBM (N.m)
Total vertical force (N)
40
35
30
25
20
15
10
50
75
100
125
150

(a)

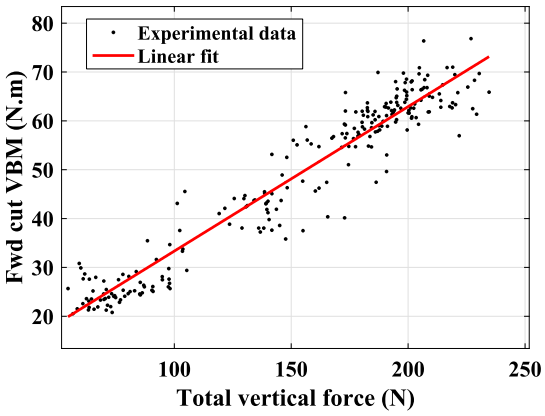
Experimental data
Linear fit
Fwd cut VBM (N.m)
Total vertical force (N)
80
70
60
50
40
30
20
100
150
200
250

(b)

Figure 19

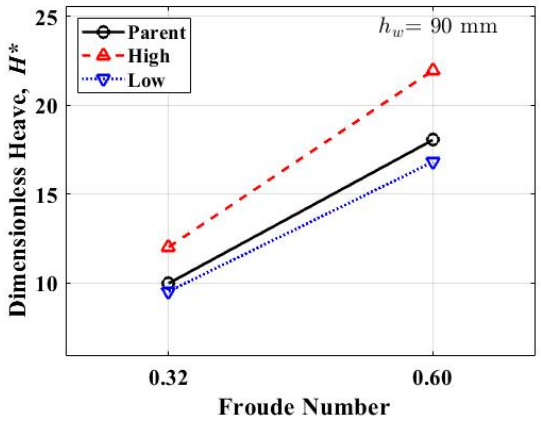

(a)

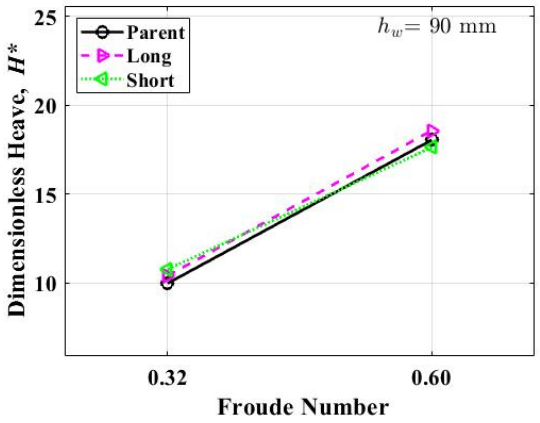

(b)

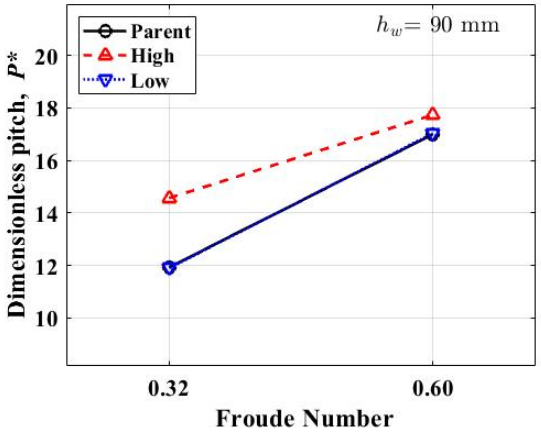

(c)

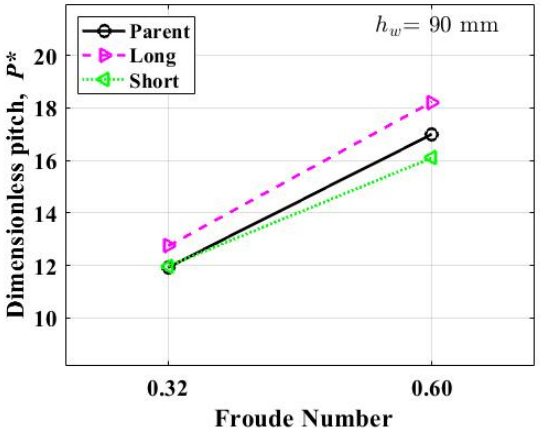

(d)

Figure 20

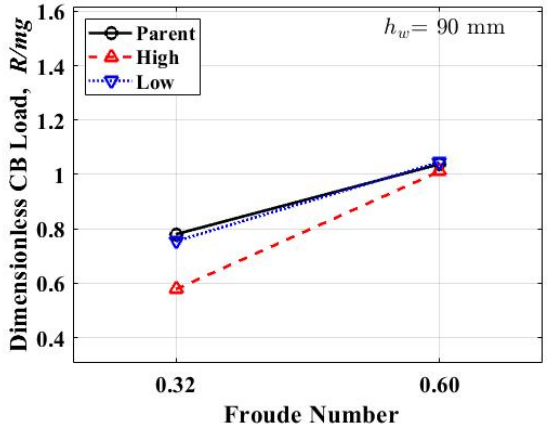

(a)

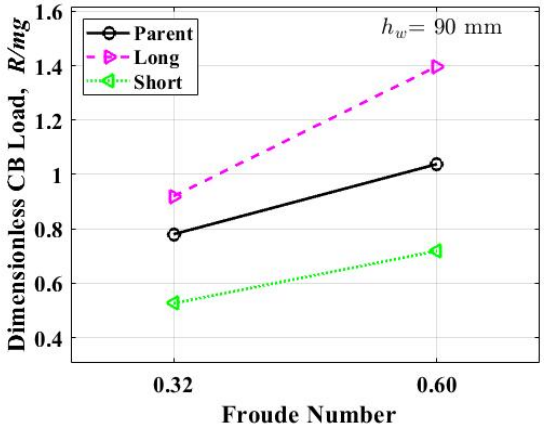

(b)

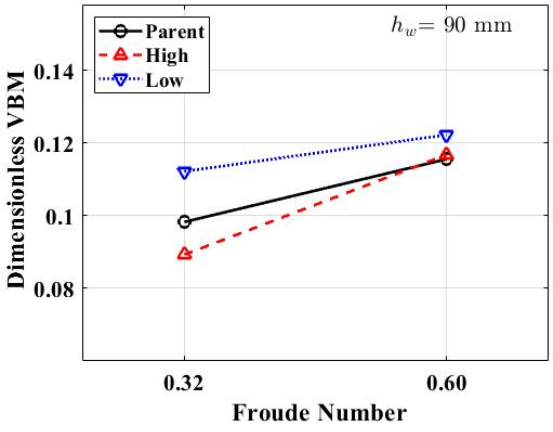

(c)

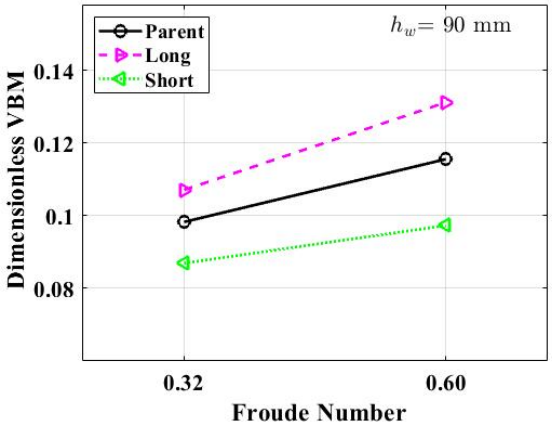

(d)

Figure Captions

Figure 1 (a) A photograph of a 112 m Incat wave piercing catamaran (Hull 067), showing the centre bow and the "jawline" labelled as ABC (b) Schematic sectional views of the Incat wave piercing catamaran from forward (left) and astern (right), showing the wet-deck flat from transom to the centre bow truncation (Incat , 2018).

Figure 2 (a) A photograph of the catamaran model (HSM02) (b) Schematic plan view of the HSM02 model showing the configuration of backbone beams and the locations of elastic links and instrumentation (LC = load cell, SG = strain gauge, A = accelerometer, LVDT = Linear Variable Differential Transformers, see Table 3 for all instrumentation details)

Figure 3 (a) A sectional representation at longitudinal position 1892 mm relative to the transom for the HSM02 model with the high, parent and low CBs-Arch top clearance is the vertical distance between the top of the arch and design waterline (b) Schematic representation of the long, parent and short centre bows of the HSM02 catamaran model

Figure 4 A schematic representation of loads and moments acting on the centre bow segment. $\boldsymbol{F_z^{aft}}$, $\boldsymbol{F_z^{fwd}}$: vertical forces measured by the aft and forward sensors, $\mathbf{F_x^{aft}}$,$\mathbf{F_x^{fwd}}$: longitudinal forces measured by the aft and forward sensors $\mathbf{T_y^{aft}}$, $\mathbf{T_y^{fwd}}$: Moments measured by the aft and forward load cells (y-axis positive direction is out of page), $\vec{\mathbf{R}}$: external force vector acting on the CB segment, $\mathbf{c_{cb}}$: the centre of gravity of the centre bow segment.

Figure 5 Sample heave and pitch time records of the catamaran model HSM02 with the parent centre bow in test condition 1 (60 mm waves, 1.53 m/s) at three different dimensionless encounter wave frequencies.

Figure 6 Dimensionless heave acceleration of the catamaran model with different bow and wet-deck configurations at a speed of 1.53 m/s in three wave heights: (a) & (d) 60 mm wave height (b) & (e) 90 mm wave height (c) 120 mm wave height

Figure 7 Dimensionless pitch acceleration of the catamaran model with different bow and wet-deck configurations at a speed of 1.53 m/s in three wave heights: (a) & (d) 60 mm wave height (b) & (e) 90 mm wave hei

Figure 8 Dimensionless vertical acceleration of the catamaran model as a function of model length for different CB configurations at $\boldsymbol{\omega_e^* \cong 4.5}$, a speed of 1.53 m/s, and in three waves heights: (a) & (d) 60 mm wave height (b) & (e) 90 mm wave height (c) 120 mm wave height

Figure 9 Photographs of the catamaran model with parent CB and wet-deck configuration in 90 mm waves at a speed of 1.53 m/s at $\boldsymbol{\omega_e^* \cong 4.53}$

Figure 10 Sample time records of CB vertical loads in 60 mm waves at $\boldsymbol{\omega_e^* \cong 4.53}$ in (a) The sum of measured loads by the aft and fwd load sensors presented as - $(\boldsymbol{F_z^{aft} + F_z^{fwd}})$ (b) The measured inertia due to CB vertical acceleration presented by $\boldsymbol{m_{cb}.a_z}$ (c) The external load $\boldsymbol{R_z}$, represented as $\boldsymbol{-(F_z^{aft} + F_z^{fwd}) + m_{cb}.a_z}$ with both 5 Hz (solid line) and 200Hz (dashed line) low pass filtered.

Figure 11 Peak total vertical force ($\boldsymbol{R_z^{peak}}$) acting on the centre bow segment of HSM02 catamaran model with different centre bows and wet-deck configurations in three different wave heights (a) & (d) 60 mm wave height (b) & (e) 90 mm wave height (c) 120 mm wave height

Figure 12 Peak total longitudinal forces ($\boldsymbol{R_x^{peak}}$) acting on the centre bow segment of HSM02 catamaran model with various centre bow lengths in two different wave heights: (a) 60 mm wave height (b) 90 mm wave height

Figure 13 Peak vertical slam forces ($\boldsymbol{F_z^{slam}}$) acting on the centre bow segment of HSM02 catamaran model with various centre bows and wet-deck configurations in three different wave heights: (a) & (b) 60 mm wave height (c) & (d) 90 mm wave height (e) 120 mm wave height

Figure 14 Peak centre bow vertical entry force ($\boldsymbol{F_z^{be}}$) of HSM02 catamaran model with various centre bows and wet-deck configurations in different speeds and wave heights

Figure 15 Sample time records of the total vertical CB load and the forward cut vertical bending moment for the parent CB at a model speed of 1.53 m/s and dimensionless wave encounter frequency of $\boldsymbol{\omega_e^* = 4.52}$ in two different wave heights (a) 60 mm waves (b) 90 mm waves.

Figure 16 Forward cut peak total sagging (positive) and hogging (negative) moments for various centre bow and wet-deck configurations at two different wave heights: (a) & (c) 60 mm wave height (b) & (d) 90 mm wave height

Figure 17 Aft cut peak total sagging (positive) and hogging (negative) moments for various centre bow and wet-deck configurations at two different wave heights: (a) & (c) 60 mm wave height (b) & (d) 90 mm wave height

Figure 18 Experimental data points (all tested wave frequencies) and linear fits describing the relationship between total vertical CB loads acting on the centre bow and forward cut vertical bending moments for the parent CB at a model speed of 1.53 m/s in two different wave heights (a) 60 mm waves (b) 90 mm waves.

Figure 19 The effect of speed on maximum dimensionless heave, H*, and pitch, P*, for various centre bow and wet-deck configurations in 90 mm waves.

Figure 20 The effect of speed on maximum dimensionless CB vertical load, ($\boldsymbol{F_z^{slam}/mg}$) , and VBM, ($\boldsymbol{VBM/mgL}$), for various centre bow and wet-deck configurations in 90 mm waves.